Evidence for weathering and volcanism during the PETM from Arctic Ocean and Peri-Tethys osmium isotope records

Alexander J. Dickson[1]*, Anthony S. Cohen[1], Angela L. Coe[1], Marc Davies[1], Ekaterina A. Shcherbinina[2] and Yuri O. Gavrilov[2].

1. Department of Environment, Earth and Ecosystems, The Open University, Walton Hall, Milton Keynes, MK7 6AA, UK.
2. Geological Institute, Russian Academy of Sciences, Pyzhevsky 7, Moscow 119017, Russian Federation.

*Corresponding author: email: alex.dickson@earth.ox.ac.uk. Telephone: +44 1865 272062. Present address: Department of Earth Sciences, University of Oxford, South Parks Road, Oxford, OX1 3AN, UK.

Keywords: Paleocene-Eocene Thermal Maximum, osmium isotopes, Arctic Ocean, Peri-Tethys, weathering, volcanism

Abstract

Sudden global warming during the Paleocene-Eocene Thermal Maximum (PETM, 55.9 Ma) occurred because of the rapid release of several thousand gigatonnes of isotopically light carbon into the oceans and atmosphere; however, the cause of this release is not well understood. Some studies have linked carbon injection to volcanic activity associated with the North Atlantic Igneous Province (NAIP), while others have emphasised carbon cycle feedbacks associated with orbital forcing. This study presents the osmium isotope compositions of mudrocks that were deposited during the PETM at four locations (one from the Arctic ocean, and three from the Peri-Tethys). The Os-isotope records all exhibit a shift of similar magnitude towards relatively radiogenic values across the PETM. This observation confirms that there was a transient, global increase in the flux of radiogenic Os from the weathering of continental rocks in response to elevated temperatures at

that time. The tectonic effects of NAIP volcanic emplacement near the onset of the PETM is recorded by anomalously radiogenic Os-isotope compositions of PETM-age Arctic Ocean samples, which indicate an interval of hydrographic restriction that can be linked tectonic uplift due to hotspot volcanism in the North Atlantic seaway. The Peri-Tethys data also document a transient, higher flux of unradiogenic osmium into the ocean near the beginning of the PETM, most likely from the weathering of young mafic rocks associated with the NAIP. These observations support the hypothesis that volcanism played a major role in triggering the cascade of environmental changes during the PETM, and highlight the influence of paleogeography on the Os isotope characteristics of marine water masses.

Introduction

There is considerable debate surrounding the source of ^{13}C-depleted carbon that was released into the oceans and atmosphere at the onset of the PETM, as well as the triggering mechanisms that could have initiated this carbon-cycle perturbation. One possibility is that orbital forcing destabilised exchangeable sources of carbon on land and in the oceans through a series of Earth-system feedback mechanisms, such as ocean and atmospheric circulation (Lourens et al., 2005, Lunt et al., 2011; De Conto et al., 2012). This hypothesis is supported by the cyclostratigraphic tuning of data from marine sedimentary sections, which suggests that early Eocene hyperthermals occurred in phase with 100 kyr orbital eccentricity cycles (Westerhold et al., 2007). This suggestion is, however, inconsistent with the observation of a difference between the phasing of the PETM relative to the 400 kyr orbital eccentricity cycle, compared to subsequent early Eocene hyperthermal events (Westerhold et al., 2007; Charles et al., 2011). An alternative hypothesis has linked the onset of the PETM to volcanic triggering associated with extensive volcanism in the North Atlantic Igneous Province (NAIP), which began ~60 Ma ago and culminated in rapid North Atlantic seafloor spreading near the Paleocene/Eocene boundary (Eldholm ad Thomas, 1993; Storey et al., 2007, 2007b). Tectonic uplift caused by the emplacement of a NAIP mantle plume at the base of the lithosphere could have caused carbon release at the start of the PETM, by triggering the dissociation of marine gas hydrates through the depressurisation of uplifted marine sediments (MacLennan and Jones, 2006), or from intermediate-depth seawater warming triggered

by tectonically-induced changes in ocean basin morphology (Bice and Marotzke, 2002; Roberts et al., 2009). A further theory suggests that the thermal alteration of organic-carbon rich marine sediments might have liberated substantial amounts of carbon by igneous intrusions during emplacement of the NAIP (Svenssen et al., 2004, 2010). However, it is difficult to test hypotheses linking the emplacement of the NAIP to the PETM using radioisotopic ages alone because the uncertainties associated with the dating of many volcanic rocks in the late Paleocene are longer than the duration of the PETM itself (Storey et al., 2007, 2007b; Svenssen et al., 2010, supplementary material).

The osmium (Os) isotope composition of seawater (expressed as $^{187}Os/^{188}Os$) reflects the mixing of radiogenic Os weathered from ancient continental crust ($^{187}Os/^{188}Os$ = ~1.4 (Peucker-Ehrenbrink and Jahn, 2001)), and unradiogenic Os from mantle (hydrothermal) and extraterrestrial sources ($^{187}Os/^{188}Os$ = 0.12 (Peucker-Ehrenbrink and Ravizza, 2000)). The residence time of Os in seawater is ~10,000-55,000 years (Burton et al, 1996; Sharma et al., 1997; Levasseur et al., 1999; Peucker-Ehrenbrink and Ravizza, 2000), which is longer than the present-day mixing time of the oceans. Seawater $^{187}Os/^{188}Os$ is therefore able to track globally-averaged variations in the proportions of radiogenic Os delivered to the oceans by the weathering of old continental rocks, and unradiogenic Os delivered by the weathering and alteration of young mafic rocks emplaced subaerially and in submarine hydrothermal systems (Pegram et al., 1992; Cohen et al., 1999; Peucker-Ehrenbrink and Ravizza, 2000). Tracing variations in weathering fluxes using Os isotopes carries the assumptions that extraterrestrial Os fluxes to the oceans are quantitatively insignificant or temporally constant, and also that the globally averaged $^{187}Os/^{188}Os$ of the radiogenic Os flux to the oceans from weathered continental rocks does not vary significantly on relatively short timescales. These assumptions are supported by previous reconstructions of global weathering fluxes using Os isotopes, which are reproducible at different locations (e.g. Cohen et al., 1999; Peucker-Ehrenbrink and Ravizza, 2001; Ravizza et al., 2001; Cohen and Coe, 2002; Cohen et al., 2004; Turgeon and Creaser, 2008; Bottini et al., 2012; Du Vivier et al., 2014). Furthermore, the relatively short seawater residence time of Os allows it to be utilised as an ocean circulation tracer in certain situations. If seawater mixing is limited in a basin or marginal seaway (for example due to topographic or hydrographic constraints), the residence time of Os in the basinal seawater may

become shorter than the global seawater Os residence time. Since Os is typically associated with organic matter (Ravizza et al., 1992; Cohen et al., 1999), enhanced organic carbon burial in restricted basins under low-oxygen conditions would favour depletion of the dissolved Os inventory in the basin seawater, which would be recorded as a decrease in sedimentary Os abundances. In such circumstances, $^{187}Os/^{188}Os$ may evolve locally to compositions that differ from the fully mixed global signal due to the greater relative importance of local Os input and output fluxes (e.g. Paquay and Ravizza, 2012).

The Os-isotope composition of seawater can be reconstructed from organic-rich mudrocks because of the high degree of enrichment of hydrogenous Os in these deposits that limits the proportional contribution from lithogenic Os (Ravizza et al., 1992; Cohen et al., 1999). Recovery of the hydrogenous Os component of sediments can be assisted by acid-leaching organic-rich mudrocks using either inverse Aqua-Regia (Cohen and Waters, 1996), or CrO_3–H_2SO_4 (Selby and Creaser, 2003). Previous studies deep-marine metalliferous clays have demonstrated a radiogenic shift in the Os-isotope composition of seawater across the PETM (Ravizza et al., 2001; Ravizza and Peuker-Ehrenbrink, 2012), but these data have never been replicated in marine mudrocks. This study presents $^{187}Os/^{188}Os$ measurements of samples from four organic-carbon enriched marine sedimentary sections spanning the PETM; three of the sections are from the northern Tethys Ocean, and the fourth is from the Arctic Ocean (Fig. 1). The intention was to assess the impact of volcanic activity on seawater $^{187}Os/^{188}Os$ during the PETM, and to investigate whether the previously observed radiogenic Os-shift across the PETM was expressed globally in a range of different marine basins.

Methods

Re-Os preparation and analyses were carried out in metal-free conditions in a Picotrace© clean laboratory using the method of Cohen and Waters (1996). 0.25-1 g of finely ground sample powder was accurately weighed into an acid-cleaned glass Carius tube, to which an exact amount of a mixed ^{185}Re-^{190}Os isotope spike and 8-12 ml of inverse Aqua Regia were added. Each sample tube was sealed with an oxygen and propane flame and placed into an oven at 180°C for 5 days. Os was extracted from the chilled acid digest with carbon tetrachloride (CCl_4), and subsequently

back extracted from CCl_4 with hydrobromic acid. Following a micro-distillation step (Birck et al., 1997), sample residues were loaded onto clean, degassed Pt filaments for analysis by n-TIMS. Instrumental mass fractionation was corrected by internal normalisation to a $^{192}Os/^{188}Os$ ratio of 3.09202. Re concentrations were determined by isotope dilution from aliquots of the same acid digests analysed for Os. Re was extracted from the inverse Aqua-Regia using an iso-amylol liquid-liquid separation technique (Birck et al., 1997). Aliquots of the purified Re solutions were doped with Ir and analysed using a Thermo-Finnegan Neptune MC-ICP-MS. Instrumental mass fractionation was corrected by normalising to a $^{193}Ir/^{191}Ir$ ratio of 1.68299 (Berglund and Wieser, 2011). All quoted $^{187}Os/^{188}Os$ ratios and Os and Re abundances were blank corrected. Average Os blanks were ~1 ppt, with an average $^{187}Os/^{188}Os$ of 0.30 (n=9). The average Re blank was ~5 ppt (n=10). Initial $^{187}Os/^{188}Os$ ratios ($^{187}Os/^{188}Os_{(i)}$) were calculated assuming a depositional age of 55.9 Ma and a Re decay constant of 1.666×10^{-11} (Smoliar et al., 1996). The uncertainty of $^{187}Os/^{188}Os_{(i)}$ has been estimated from separate digestions of an in-house mudrock standard (Monterey mudrock 00N118) as ± 0.015 (2 S.D., n=8).

Results

The stratigraphy of the Peri-Tethys Ocean records have been discussed in detail by Gavrilov et al. (2003) and Dickson et al. (2014). All sites contain mudrocks variably enriched in organic carbon by up to ~18 wt%. These mudrocks were deposited during a negative $\delta^{13}C_{org}$ excursion of ~4‰ (Dickson et al., 2014), which can be attributed to isotopically light carbon release during the PETM. These features, together with primary biostratigraphic constraints at each site from nannofossil and dinocyst taxonomy, allow the sections to be correlated (Fig. 2).

^{192}Os concentrations in all samples are greatly elevated above the average crustal concentration (Peucker-Ehrenbrink and Jahn, 2001). At Kheu River and Guru-Fatima, $^{187}Os/^{188}Os_{(i)}$ increases from ~0.32 below the CIE to a maximum of 0.38–0.39 during the CIE. $^{187}Os/^{188}Os_{(i)}$ values at Dzhengutay also increase to 0.39 within the CIE with a similar overall range to the other Tethys sites. The $^{187}Os/^{188}Os_{(i)}$ records from Kheu River and Guru Fatima also display shifts to relatively unradiogenic values near the base of the CIE. The lowest $^{187}Os/^{188}Os_{(i)}$ at both Guru-Fatima and Kheu River occur immediately after the first $\delta^{13}C_{org}$ data point indicating the PETM CIE.

However, fully deciphering the phasing of these lead-lag relationships is limited by the temporal resolution of each record, which is relatively low over the CIE onset due to the limited availability of sample material.

There is an increase in $^{187}Os/^{188}Os_{(i)}$ of Arctic Ocean seawater from 0.39 to 0.55 during the PETM, which occurs at 390.66 mcd, 4.5 m below the first negative shift in $\delta^{13}C_{org}$ that is taken to denote the onset of the CIE (Sluijs et al., 2006; Stein et al, 2006; Dickson et al., 2012). As with the Tethys Ocean sites, the relatively radiogenic Arctic Ocean $^{187}Os/^{188}Os_{(i)}$ recorded at Site M0004A returns to less radiogenic values above the PETM.

Discussion

Data integrity

The high ^{192}Os concentrations in most of the samples confirm a substantial enrichment of hydrogenous Os over the average continental crust (detrital Os) contribution. Furthermore, the Re-Os data for each of the four sites are generally tightly clustered around an isochron age of 55.9 Ma (Fig. 3). Large differences in the contribution of lithogenic Os to the measured $^{187}Os/^{188}Os$ ratios, or a significant amount of post-depositional remobilisation of Re or Os, would impart a greater degree of scatter to the plots (e.g. Peucker-Ehrenbrink and Hannagan, 2000; Jaffe et al., 2002; Georgiev et al., 2012) than is observed. In the case of the three Tethys sites, the Re-Os data from the PETM intervals define identical $^{187}Os/^{188}Os_{(i)}$ of 0.36, further demonstrating the robustness of the datasets and showing that each location sampled the same, well-mixed late Paleocene−early Eocene seawater Os reservoir. It is noteworthy that the steady-state $^{187}Os/^{188}Os_{(i)}$ of Peri-Tethys seawater of 0.36 inferred from Fig. 3 is extremely close to the pre- and post-PETM $^{187}Os/^{188}Os$ values measured for open ocean seawater at DSDP Site 213 and 549 (Ravizza et al., 2001). This observation implies that that there was little or no hydrographic restriction in the northern Peri-Tethys and that the study locations were able to freely exchange seawater with the wider Tethys Ocean. These lines of evidence demonstrate that the new data are robust and that variations in $^{187}Os/^{188}Os_{(i)}$ at each site can be used to track variations in the Os-isotope compositions of early Eocene seawater.

175 *Weathering of radiogenic Os during the PETM*

176 All four studied sections exhibit a shift towards toward more radiogenic $^{187}Os/^{188}Os$ values during
177 the PETM CIE, with the Tethys sites having similar magnitude shifts of ~0.06. The range of the
178 $^{187}Os/^{188}Os_{(i)}$ excursions recorded at the three Tethys Ocean sites are similar to the magnitude of
179 the shift towards more radiogenic $^{187}Os/^{188}Os$ values during the PETM at DSDP Sites 213 and 549
180 in the Indian Ocean and North Atlantic Ocean respectively (Ravizza et al., 2001), at Zumaya in
181 Spain (Schmitz et al., 2004), and also in Pacific Ocean Fe-Mn crusts (Klemm et al., 2005)
182 (supplementary online material). The Site 549 data (Ravizza et al., 2001; Peucker-Ehrenbrink and
183 Ravizza, 2012) are systematically slightly higher than the Tethys Ocean datasets, which may be
184 due to the leaching of small quantities of lithogenic Os from the clay-rich deposits at that site.
185 Likewise, Arctic Ocean $^{187}Os/^{188}Os_{(i)}$ values recorded at Site M0004A are also systematically higher
186 than at the Tethys Ocean sites, which is consistent with a range of observations suggesting that
187 seawater exchange between the Arctic Basin and global ocean occurred at a rate that was too
188 slow to allow the $^{187}Os/^{188}Os$ of Arctic Ocean seawater to equilibrate fully with the global ocean
189 during the portion of the late Paleocene and early Eocene studied. Nontheless, the consistent
190 observation of relatively more radiogenic $^{187}Os/^{188}Os$ during the CIE at the different locations leads
191 us to conclude that the Os-isotope records (Fig. 2) reflect a shift in the $^{187}Os/^{188}Os$ of global
192 seawater towards relatively radiogenic values during the PETM. This observation requires a
193 change in the global balance and/or composition of Os fluxes to the ocean across this event
194 (Ravizza et al., 2001; Cohen et al., 2007).

195 The overall increase in seawater $^{187}Os/^{188}Os$ during the PETM could have been caused by
196 an increase in the flux to the oceans of radiogenic Os weathered from continental rocks, by an
197 increase in the average $^{187}Os/^{188}Os$ of weathered continental rocks, or by a decrease in the flux of
198 unradiogenic Os to seawater. An increase in the flux of continentally-derived Os at a global scale is
199 the most parsimonious interpretation of the data in the light of evidence for a perturbed
200 hydrological cycle during the PETM (Bowen et al., 2004; Pagani et al., 2006; Handley et al., 2012)
201 and for exceptionally high fluxes of terrestrial sediments to continental margins (Schmitz and
202 Pujalte, 2007; Sluijs et al., 2008a; John et al., 2008; Dickson et al., 2014). In principle, the shift
203 could also have been caused by the preferential weathering of radiogenic Os from exposed

organic-rich mudrocks, thereby raising the average $^{187}Os/^{188}Os$ of weathering fluxes. However, there is no evidence for a change in the terrestrial exposure of such deposits during the PETM. Additionally, Svensen et al. (2004, 2010) have suggested that hydrothermal fluids could have been expelled rapidly into the Vøring and Møre basins (northeast Atlantic Ocean) at the onset of the PETM after the heating by igneous intrusions of Cretaceous mudrocks, which are likely to have had more radiogenic $^{187}Os/^{188}Os$ than early Eocene seawater (Ravizza et al., 2007; Turgeon and Creaser, 2008; Bottini et al., 2012). However, assuming a seawater residence time for Os of ~10^4 years, and a duration for the PETM of 10^5 years (Röhl et al., 2007; Charles et al., 2011) the PETM $^{187}Os/^{188}Os$ records obtained here and in previous studies (Ravizza et al., 2001; Peucker-Ehrenbrink and Ravizza, 2012) require the flux of radiogenic Os to be sustained over multiple residence times to explain the prolonged excursion to more radiogenic seawater $^{187}Os/^{188}Os$ values (Röhl et al., 2007; Charles et al., 2011). The prolonged duration for the radiogenic $^{187}Os/^{188}Os$ excursion is therefore incompatible with the very short timescale for the postulated hydrothermal fluid release of only a few thousand years (Svensen et al., 2004).

At steady state, the Os-isotope composition of seawater can be described by mixing between unradiogenic and radiogenic Os input fluxes. The endmember $^{187}Os/^{188}Os$ compositions of these fluxes are assumed to be 0.12 and 1.4 respectively (Luck and Allègre, 1983; Peucker-Ehrenbrink and Jahn, 2001). The relative contribution (mole fraction, F) of the radiogenic endmember can be described by:

$$F_r = (R_s - R_u) / (R_r - R_u) \quad (1)$$

Where subscripts *r, s* and *u* denote the radiogenic, seawater and unradiogenic $^{187}Os/^{188}Os$ compositions respectively (Ravizza et al., 2001). The contribution of the unradiogenic endmember can then be calculated using:

$$F_u = (1 - F_r) \quad (2)$$

The fractional increase in radiogenic Os fluxes during the PETM has been calculated with the assumption that flux of unradiogenic Os to the oceans remained constant. Then, the fractional increase in the radiogenic contribution (ΔF_r) can be calculated:

$$\Delta F_r = ((F_{u\ [\text{pre-event}]} / F_{u\ [\text{event}]}) - F_{u\ [pre\text{-}event]}) / F_{r\ [\text{pre-event}]} \quad (3)$$

Applying this approach to data from the best resolved Peri-Tethys site (Kheu River), yields a result suggesting a 38% increase in the flux of radiogenic Os for the PETM compared with pre-PETM fluxes. The magnitude of the increase in $^{187}Os/^{188}Os_{(i)}$ during the PETM at Guru-Fatima is higher than at Kheu River, but is based on a single $^{187}Os/^{188}Os_{(i)}$ measurement of 0.43 during the CIE. A similar calculation can not be made for Dzhengutay because pre-PETM samples are not available. For comparison, the calculated change in radiogenic Os flux during the PETM based on the DSDP Site 549 dataset (Ravizza et al., 2001) suggests an increase in radiogenic Os flux of 44%, which is very close to our estimate using data from the Tethyan Kheu River site. The fact that $^{187}Os/^{188}Os_{(i)}$ closely tracks the evolution of the CIE during the PETM is consistent with a mechanistic link between elevated global temperatures, moisture availability and weathering fluxes (Gaillardet et al. 1999), as also inferred for other global warming events in Earth history (e.g. Ravizza et al., 2001; Cohen and Coe, 2002; Cohen et al., 2004; Pagani et al., 2006; Bottini et al., 2012; Pogge van Strandmann et al., 2013).

Unradiogenic Os fluxes near the beginning of the PETM

Our records contain two key lines of evidence for a phase of volcanism at the onset of the PETM. The first is the short-term transient decrease in $^{187}Os/^{188}Os_{(i)}$ of ~0.05 near the base of the CIE at Kheu River and Guru-Fatima (Fig. 4) (the behaviour of $^{187}Os/^{188}Os_{(i)}$ at the onset of the PETM is unknown at Dzhengutay, because samples from the lower part of that section were not sampled). The similarity between the observed $^{187}Os/^{188}Os_{(i)}$ decrease in the two Peri-Tethys sites with a previously observed decrease in $^{187}Os/^{188}Os$ at the base of the PETM at Zumaya, Spain (Schmitz et al., 2004), suggests that the decrease in $^{187}Os/^{188}Os$ was likely to have been at least a regional phenomenon. The timings of the $^{187}Os/^{188}Os$ decrease at each site are consistent, beginning near

261 the base of the negative $\delta^{13}C_{org}$ excursion, and ending within nannofossil zone NP 9 (Fig. 3).
262 These features constrain the duration of the transient stratigraphic shift in $^{187}Os/^{188}Os$ to a few tens
263 of thousands of years at most (Charles et al., 2011). The $^{187}Os/^{188}Os$ decrease at the start of the
264 PETM is consistent with a proportionally larger flux of unradiogenic Os to the oceans near the start
265 of the PETM. Equation (3) was used to calculate the magnitude of the unradiogenic flux increases
266 recorded in the initial stages of the PETM (Fig. 3), but substituting F_u *for* F_r and vice-versa. This
267 calculation resulted in fluxes of unradiogenic Os for Kheu River, Guru Fatima and Zumaya that
268 were 33%, 39% and 12% higher, respectively, compared to pre-excursion fluxes.
269 There is no convincing evidence for an extraterrestrial impact in PETM deposits that could
270 explain the shift towards relatively unradiogenic $^{187}Os/^{188}Os$ at the start of the PETM (Schmitz et
271 al., 2004). However, a recent $^{187}Os/^{188}Os$ record from the Svalbard Central Basin (core BH9/04)
272 suggests that a large amount of volcanic ash was deposited in the Central basin over an interval of
273 approximately 8000 years shortly before the onset of the PETM (Fig. 4, Weiczorek et al., 2013).
274 The magnitude of the unradiogenic Os-isotope excursion in the Central Basin is about six times
275 larger than in the Tethys sections, probably because the proximity of that site made it sensitive to
276 the direct input of unradiogenic Os from mafic material (ash) from the NAIP. It is noteworthy that
277 the $^{187}Re/^{188}Os$ and $^{187}Os/^{188}Os$ data from Svalbard (Weiczorek et al., 2013) exhibit a high degree
278 of scatter when examined around a 55.9 Ma reference isochron. In contrast, the new Tethys
279 records reported here have $^{187}Re/^{188}Os$ and $^{187}Os/^{188}Os$ data that are more tightly defined around
280 55.9 Ma isochrons (Fig. 3). These observations confirm that the addition of unradiogenic Os to
281 Svalbard sediments, as identified by Weiczorek et al. (2013), was more than a regional-scale
282 phenomenon, and that volcanism caused a significant (although locally disproportionate) impact on
283 the Os-isotope composition of global seawater during the early stages of the PETM.
284 The second line of evidence for volcanism near the onset of the PETM comes from the
285 sharp increase in the $^{187}Os/^{188}Os_{(i)}$ of Arctic Ocean seawater below the onset of the PETM at Site
286 M0004A that is not observed in a similar stratigraphic position at any site outside the Arctic Basin
287 (Fig. 2). This shift is interpreted to record a short interval (between 390.66−388.63 mcd) when
288 hydrological restriction became sufficiently pronounced so as to cause the $^{187}Os/^{188}Os$ of Arctic
289 Ocean seawater to evolve independently from the global seawater trend. Taking the age of the

PETM onset and the age of the C25n/C24r magnetic reversal from Westerhold et al. (2008), the approximate timing of hydrographic restriction in the Arctic Ocean can be estimated to have occurred ~50-500 kyr prior to the onset of the CIE. The broad range of estimates is partly the result of a paucity of age-control between the C25n/C24r reversal and the PETM (Backman et al., 2008), along with incomplete recovery of the PETM interval itself, which makes identification of the CIE onset highly imprecise (±0.9 m). The relative ages noted here should therefore be treated with a degree of caution.

The temporary period of pronounced hydrographic restriction at Site M0004A is consistent with low sedimentary Mo/U ratios and very low $\delta^{98/95}$Mo (Dickson et al., 2012). The abrupt increase in $^{187}Os/^{188}Os_{(i)}$ is unlikely to have been caused by an increase in the delivery of radiogenic Os to the Arctic Ocean from surrounding landmasses, because proxy data for moisture availability and continental temperatures do not show significant changes in pan-Arctic temperatures or hydrology before the onset of the CIE (Fig. 2, supplementary information) (Pagani et al., 2006; Weijers et al., 2007). The most likely explanation for the increase in the $^{187}Os/^{188}Os$ of Arctic Ocean seawater is therefore a reduction in the flux of less radiogenic Os into the Arctic Basin from the global ocean, as hydrological restriction in the basin became more pronounced (Fig. 1).

The temporary period of marked hydrological restriction in the Arctic Ocean preceding the onset of the PETM could have been caused by the tectonic uplift of the North Atlantic seaway. Evidence suggesting a regional relative sea-level (RSL) fall of >200 m is associated with the Lamba/Flett sequence boundary in the Faroe-Shetland Basin and the Lista IIIb/Forties sequence boundary in the North Sea (Mudge and Bujak, 2001; Smallwood and Gill, 2002), the ages of which are constrained by the highest occurrence of the dinocyst *Alisocysta margarita* and the lowest occurrence of *Apectodinium augustum* (Mudge and Bujak, 2001). This RSL fall has been attributed to regional mantle-plume related uplift, lithospheric thinning and the commencement of an active period of NAIP volcanism (MacLennan and Jones, 2006; Smallwood and Gill, 2002). A fall in eustatic sea-level of several tens of metres, deduced from the sequence boundary on the New Jersey shelf, in New Zealand, and in the Tethys Ocean (Gavrilov et al., 2003; Sluijs et al., 2008b; Harding et al., 2011), is likely to have further contributed to the change in RSL, but cannot account for its full magnitude.

318 The timing of RSL fall in the North Atlantic seaway (Sluijs et al., 2008b) is consistent with
319 available age constraints at Site M0004A (Expedition 302 Scientists, 2006; Backman et al., 2008)
320 for the onset of enhanced hydrological restriction in the Arctic Ocean inferred from our Os-isotope
321 record (Fig. 2). It is likely that seawater exchange across the North Atlantic seaway was limited
322 throughout the PETM, since re-flooding took place after the last occurrence of the dinocyst
323 *Cerodinium wardense* (Mudge and Bujak, 2001), which occurs stratigraphically above the PETM in
324 Site M0004A (Expedition 302 Scientists, 2006). A slight alleviation of hydrographic restriction in the
325 Arctic basin at the minimum of the CIE (Dickson et al., 2012) was probably facilitated by a eustatic
326 sea-level rise of 20-30 m at the onset of the PETM (Gavrilov et al., 2003; Sluijs et al., 2008b;
327 Harding et al., 2011) that deepened the Arctic-Tethys connection through the central Asian Turgay
328 Straits (Fig. 1). Seawater exchange through this seaway would have been slow enough to maintain
329 a small difference between seawater $^{187}Os/^{188}Os$ within the Arctic Basin and the $^{187}Os/^{188}Os$ of the
330 global ocean (Fig. 2), but was sufficiently voluminous for Arctic Ocean seawater $\delta^{98/95}Mo$ to record
331 the global seawater $\delta^{98/95}Mo$ (Dickson et al., 2012). This difference in isotopic responses arises
332 because the residence time of Mo in seawater is approximately an order of magnitude longer than
333 for Os, and thus would require an almost complete cessation of seawater exchange before the
334 $\delta^{98/95}Mo$ of Arctic Ocean seawater could begin to evolve independently from that of the global
335 ocean.
336 It has been suggested that multiple sources of carbon could be necessary to reconcile
337 observations of carbonate dissolution and the shape and magnitude of the PETM CIE (Zeebe et
338 al., 2004; Dunkley-Jones et al., 2010; Carozza et al., 2011). Tectonic uplift of the North Atlantic
339 seaway by NAIP volcanic activity could have altered North Atlantic Ocean circulation, generating
340 warming at intermediate depths sufficient to destabilise gas hydrates buried in marine sediments
341 (Lunt et al., 2011, Bice and Marotzke, 2002; Roberts et al., 2009; Sluijs et al., 2007). This scenario
342 requires a time lag of at least several thousand years between the emergence of the North Atlantic
343 seaway and the release of additional fossil carbon, and is consistent with the commencement of
344 Arctic Basin restriction prior to the onset of the PETM observed at Site M0004A. A key test of this
345 hypothesis will be the recovery of a complete PETM section from the Arctic Ocean by future
346 drilling.

Conclusions

The new Os-isotope data presented here from the Peri-Tethys and Arctic Ocean sites all exhibit a small increase towards more radiogenic Os-isotope values during the PETM, reflecting a proportional increase in the flux of radiogenic Os to the oceans in response to elevated continental weathering rates. The data also indicate that seawater $^{187}Os/^{188}Os$ became relatively unradiogenic for a short interval of time either at, or slightly before the onset of the PETM. Together with evidence for enhanced hydrological restriction in the Arctic Basin in response to the emplacement of the NAIP, these data strongly support the hypothesis that volcanism triggered the carbon-cycle feedbacks that caused rapid global warming and environmental change during the PETM (Eldholm and Thomas, 1993; Svensen et al., 2004; MacLennan and Jones, 2006; Cohen et al., 2007; Storey et al., 2007; Du Vivier et al., 2012; Weiczorek et al., 2013). Lastly, the new results show that there were clear differences between the Os-isotope compositions of seawater in the Arctic basin and in the global ocean during the early Eocene. Since restricted basins, such as the Arctic, are inherently prone to forming organic-rich mudrock deposits, these observations reinforce the importance (e.g. Dickson et al., 2012, 2014b) of understanding the original depositional and hydrographic setting of the deposits before inferences about global seawater chemistry can be made (e.g. Paquay and Ravizza, 2012; Du Vivier et al., 2012).

Acknowledgements

The Integrated Ocean Drilling Program provided sample material. This study was funded by the Natural Environment Research Council (NE/F021313/1) and supported by the Open University. Manuela Fehr is thanked for laboratory support. The manuscript was improved by constructive reviews from Tom Dunkley-Jones, Dave Selby and one anonymous reviewer.

References

Backman, J., Jakobsson, M., Frank, M., Sangiorgi, F., Brinkhuis, H., Stickley, C., O'Regan, M., Lvlie, R., Spofforth, D., Gattacecca, J., Moran, K., King, J. and Heil, C. (2008) Age model and core-

375 seismic integration for the Cenozoic Arctic Coring Expedition sediments from the Lomonosov
376 Ridge. Paleoceanography 23, PA1S03, doi:10.1029/2007PA001476.
377
378 Berglund, M. and Weiser, M.E. (2011), Isotopic compositions of the elements 2009 (IUPAC
379 technical report). Pure Appl. Chem. 83(2), 397-410.
380
381 Bice, K.L. and Marotzke, J., (2002) Could changing ocean circulation have destabilised methane
382 hydrate at the Paleocene/Eocene boundary? Paleoceanography 17, 1018,
383 10.1029/2001PA000678.
384
385 Birck, J.L., Roy Barman, M., Capmas, F. (1997) Re-Os isotopic measurements at the femtomole
386 level in natural samples. Geostan. Newslett. 20, 19-27.
387
388 Bottini, C., Cohen, A.S., Erba, E., Jenkyns, H. and Coe, A.L. (2012) Osmium-isotope evidence for
389 volcanism, weathering, and ocean mixing during early Aptian OAE 1a. Geology 40, 583-586.
390
391 Bowen, G.J., Beerling, D.J., Koch, P.L., Zachos, J.C. and Quattlebaum, T. (2004) A humid climate
392 state during the Palaeocene/Eocene Thermal Maximum. Nature 432, 495-499.
393
394 Burton, K.W., Bourdon, E., Birck, J-L., Allegre, A.L. and Hein, J.R. (1999) Osmium isotope
395 variations in the oceans recorded by Fe-Mn crusts. Earth Planet. Sci. Lett. 171, 185-197.
396
397 Charles, A.J., Condon, D.J., Harding, I.C., Pälike, H., Marshall, J.E.A., Cui, Y., Kump, L. and
398 Croudace, I.W. (2011) Constraints on the numerical age of the Paleocene-Eocene boundary.
399 Geochem. Geophys. Geosyst. 12(6), Q0AA17, doi:10.1029/2010GC003426 .
400
401 Cohen, A.S. and Coe, A.L. (2002), New geochemical evidence for the onset of volcanism in the
402 Central Atlantic magmatic province and environmental change at the Triassic-Jurassic boundary.
403 Geology 30, 267-270.

Cohen, A.S., Coe, A.L., Bartlett, J.M. and Hawksworth, C.J. (1999) Precise Re-Os ages of organic-rich mudrocks and the Os-isotope composition of Jurassic seawater. Earth Planet. Sci. Lett.167, 159-173.

Cohen, A.S., Coe, A.L., Harding, S.M. and Schwark, L. (2004) Osmium isotope evidence for the regulation of atmospheric CO_2 by continental weathering. Geology 32, 157-160.

Cohen, A.S., Waters, F.G. (1996) Separation of osmium from geological materials by solvent extraction for analysis by thermal ionisation mass spectrometry. Anal. Chim. Acta, 332, 267-275.

Cohen, A.S., Coe, A.L. and Kemp, D.K. (2007), The late Palaeocene–early Eocene and Toarcian (Early Jurassic) carbon isotope excursions: a comparison of their time scales, associated environmental changes, causes and consequences. J Geological Soc. Lon. 164, 1093-1108.

DeConto, R.M., Galeotti, S., Pagani, M., Schafer, K., Zhang, T., Pollard, D. and Beerling, D.J. (2012) Past extreme warming events linked to massive carbon release from thawing permafrost. Nature 484, 87-91.

Dickson, A.J., Cohen, A.S. and Coe, A.L., (2012) Seawater oxygenation during the Paleocene Eocene Thermal Maximum, Geology 40, 639-642.

Dickson, A.J., Rees-Owen, R., März, C., Coe, A.L., Cohen, A.S., Pancost, R.D., Taylor, K. and Shcherbinina, E. (2014) The spread of marine anoxia on the northern Tethys margin during the Paleocene Eocene Thermal Maximum. *Paleoceanography* 29: 471-488.

Dickson, AJ, Cohen, AS, Coe, AL (2014b) Continental margin molybdenum isotope signatures from the early Eocene. *Earth Planet. Sci. Lett.* 404: 389-395.

433 Du Vivier, A.D.C., Selby, D., Sageman, B.B., Jarvis, I., Gröcke, D.R., and Voigt, S. (2014) Marine
434 187Os/188Os isotope stratigraphy reveals the interaction of volcanism and ocean circulation
435 during Oceanic Anoxic Event 2. *Earth Planet. Sci. Lett.* 389: 23-33.
436
437 Eldholm, O. and Thomas, E. (1993) Environmental impact of volcanic margin formation. *Earth*
438 *Planet. Sci. Lett.* 117: 319-329.
439
440 Expedition 302 Scientists (2006) Sites M0001-M0004. *Proc. IODP, 302*, eds Backman, J et al,
441 (Edinburgh), doi:10.2204/iodp/proc.302.104.2006.
442
443 Gaillardet, J., Dupré, B., Louvat, P. and Allègre, A.J. (1999), Global silicate weathering and CO_2
444 consumption rates deduced from the chemistry or large rivers. Chem. Geol. 159, 3–30.
445
446 Gavrilov, Y., Schcerbinina, E., Golovanova, O. and Porovsky, B. in Climatic and biotic events of the
447 Paleogene (CBEP 2009), extended abstracts from an international conference in Wellington, New
448 Zealand (eds. Crouch, E.M., Strong, C.P. and Hollis, C.J.) 67-70 (GNS Science Miscellaneous
449 Series 18, 2009).
450
451 Gavrilov, Y.O., Shcherbinina, E.A. and Oberhansli, H., (2003) Paleocene-Eocene boundary events
452 in the northeastern Peri-Tethys. In Wing, S.L., Gingerich, P.D., Schmitz, B. and Thomas, E. (eds.),
453 Causes and consequences of globally warm climates in the early Paleogene. Boulder, Colorado.
454 GSA Special Paper 369, 147-168.
455
456 Georgiev, S., Stein, H.J., Hannah, J.L., Weiss, H.M., Bingen, B., Xu, G., Rein, E., Hatlø, V.,
457 Løseth, H., Nali, M. and Piasecki, S. (2012), Chemical signals for oxidative weathering predict Re-
458 Os isochroneity in black shales, East Greenland. Chemical Geology 324-325, 108-121.
459
460 Harding, I.C., Charles, A.J., Marshall, J.E.A., Plike, H., Roberts, A.P., Wilson, P.A., Jarvis, E.,
461 Thorne, R., Morris, E., Moremon, R., Pearce, R.B. and Akbari, S. (2011) Sea-level and salinity

462 fluctuations during the Paleocene-Eocene thermal maximum in Arctic Spitsbergen. Earth Planet.
463 Sci. Lett. 303, 97-107.
464
465 Jaffe, L.A., Peucker-Ehrenbrink, B. and Petsch, S.T. (2002), Mobility of rhenium, platinum group
466 elements and carbon during black shale weathering. Earth Plant. Sci. Lett. 198, 339-353.
467
468 John, C.M., Bohaty, S.M., Zachos, J.C., Sluijs, A., Gibbs, S., Brinkhuis, H. and Bralower, T. J.,
469 (2008) North American continental margin records of the Paleocene-Eocene thermal maximum:
470 implications for global carbon and hydrological cycling. Paleoceanography 23, PA2217,
471 doi:10.1029/2007PA001465.
472
473 Klemm, V., Levasseur, S., Frank, M., Hein, J.R. and Halliday, A.N. (2005) Osmium isotope
474 stratigraphy of a marine ferromanganese crust. Earth Planet Sci. Lett. 238, 42-48.
475
476 Küspert, W (1982) Environmental change during oil shale deposition as deduced from stable
477 isotope ratios. Cyclic and event stratification, eds Einsele, S, Seilacher, A. (Springer, New York),
478 pp 482-501.
479
480 Levasseur, S., Birck, J-L. and Allegre, C.J., (1999) The osmium riverine flux and the oceanic mass
481 balance of osmium. Earth Planet. Sci. Lett. 174, 7-23.
482
483 Lourens, L.J., Sluijs, A., Kroon, D., Zachos, J.C., Thomas, E., Röhl, U., Bowles, J. and Raffi, I.,
484 (2005) Astronomical pacing of late Palaeocene to early Eocene global warming events, Nature
485 435, 1083-1087.
486
487 Lunt, D.J., Ridgwell, A., Sluijs, A., Zachos, J., Hunter, S. and Haywood, A. (2011) A model for
488 orbital pacing of methane hydrate destabilisation during the Palaeogene. Nature Geoscience 4,
489 775-778.
490

MacLennan, J. and Jones, S.M. (2006) Regional uplift, hydrate dissociation and the origins of the Paleocene-Eocene Thermal Maximum. Earth Planet. Sci. Lett. 245, 65-80.

Mudge, D.C. and Bujak, J.P. (2001) Biostratigraphic evidence for evolving palaeoenvironments in the lower Paleogene of the Faroe-Shetland Basin. Mar. Pet. Geol. 18, 577-590.

Nisbet, E.G., Jones, S.M., MacLennan, J., Eagles, G., Moed, J., Warwick, N, Bekki, S., Braesicke, P., Pyle, J.A. and Fowler, C.M.R. (2009) Kick-starting ancient warming. Nature Geoscience 2, 156-159.

Pagani, M., Pedentchouk, N., Huber, M., Sluijs, A., Schouten, S., Brinkhuis, H., Sinninghe Damste, J.S., Dickens, G.R. and Expeditions 302 Scientists (2006) Arctic hydrology during global warming at the Paleocene/Eocene thermal maximum. Nature 442, 671-675.

Paquay, F.S. and Ravizza, G. (2012), Heterogeneous seawater $^{187}Os/^{188}Os$ during the late Pleistocene glaciations. Earth Planet. Sci. Lett. 349-350, 126-138.

Pegram, W.J., Krishnaswami, S., Ravizza, G.E. and Turekian, K.K. (1992) The record of sea water $^{187}Os/^{186}Os$ variation through the Cenozoic. Earth Planet. Sci. Lett. 113, 560-576.

Peucker-Ehrenbrink, B. and Hannigan, R.E. (2000), Effects of black shale weathering on the mobility of rhenium and platinum group elements. Geology 28, 475-478.

Peucker-Ehrenbrink, B. and Jahn, B.M. (2001) Rhenium-osmium isotope systematics and platinum-group elements concentrations: loess and the upper continental crust. Geochem. Geophys. Geosyst. 2, 1061, doi:10.1029/2001GC000172.

Peucker-Ehrenbrink, B. and Ravizza, G. (2012) Osmium isotope stratigraphy, in The Geologic Time Scale 2012 (eds Gradstein, F. Ogg, J., Schmitz, M. and Ogg, G.) 145-166 (Elsevier, 2012).

Peucker-Ehrenbrink, B. and Ravizza, G. (2000) The marine osmium isotope record. Terra Nova 12, 205-219 (2000).

Pogge van Strandmann, P.A.E., Jenkyns, H.C. and Woodfine, R.G. (2013) Lithium isotope evidence for enhanced weathering during Oceanic Anoxic Event 2. Nature Geoscience 6, 668-672.

Roberts, C.D., LeGrande, A.N and Tripati, A.K. (2009) Climate sensitivity to Arctic seaway restriction during the early Paleogene. Earth Planet. Sci. Lett. 286, 576-585.

Ravizza, G. (2007) Reconstructing the marine 187Os/188Os record and the particulate flux of meteoric osmium during the late Cretaceous. Geochim. Cosmochim. Acta 71, 1355-1369.

Ravizza, G., Norris, R.N., Blusztajn, J. and Aubry, M-P. (2001) An osmium isotope excursion associated with the late Paleocene Thermal Maximum: evidence of intensified chemical weathering. Paleoceanography 16, 155-163.

Schmitz, B., Peucker-Ehrenbrink, B., Heilmann-Clausen, C., Åberg, G., Asaro, F. and Lee, C-T. A., (2004) Basaltic explosive volcanism, but no comet impact, at the Paleocene-Eocene boundary: high-resolution chemical and isotopic records from Egypt, Spain and Denmark. Earth Planet. Sci. Lett. 225, 1-17.

Schmitz, B. and Pujalte, V. (2007) Abrupt increase in seasonal extreme precipitation at the Paleocene-Eocene boundary. Geology 35, 215-218.

Sharma, M.,Papanastassiou, D.A. and Wasserburg, G.J. (1997) The concentration and isotopic composition of osmium in the oceans. Geochim. Cosmochim. Acta 61, 3287-3299.

548 Sluijs, A., Brinkhuis, H., Schouten, S., Bohaty, S.M., John, C.M., Zachos, J.C., Reichart, G-J.,
549 Sinninghe Damste, J.S., Crouch, E.M. and Dickens, G.R. (2007) Environmental precursors to rapid
550 light carbon injection at the Paleocene/Eocene boundary. Nature 450, 1218-1221.
551
552 Sluiis, A., Röhl, U., Schouten, S., Brumsack, H-J., Sangiorgi, F., Sinninghe Damste, J.S. and
553 Brinkhuis, H. (2006) Subtropical Arctic Ocean temperatures during the Palaeocene/Eocene
554 thermal maximum. Nature 441, 610-613.
555
556 Sluiis, A., Schouten, S., Pagani, M., Woltering, M., Brinkhuis, H., Sinninghe Damste, J.S., Dickens,
557 G.R., Huber, M., Reichart, G-J., Stein, R., Matthiessen, J., Lourens, L., Pedentchouk, N.,
558 Backman, J., Moran, K. and Expedition 302 Scientists (2006) Arctic late Paleocene-early Eocene
559 palaeoenvironments with special emphasis on the Paleocene-Eocene thermal maximum
560 (Lomonosov Ridge, Integrated Ocean Drilling Program Expedition 302). Paleoceanography 23,
561 PA1S11, doi:10.1029/2007PA001495 (2008a).
562
563 Sluijs, A., Brinkhuis, H., Crouch, E., John, C.M., Handley, L., Munsterman, D., Bohaty, S.M.,
564 Zachos, J.C., Reichart, G-J., Schouten, S., Pancost, R.D., Sinninghe Damste, J.S., Welters,
565 N.L.D., Lotter, A.F. and Dickens, G.R. (2008a) Eustatic variations during the Paleocene-Eocene
566 greenhouse world. Paleoceanography 23, PA4216, doi:10.1029/2008PA001615 (2008b).
567
568 Smallwood, J.R. and Gill, C.E. (2002) The rise and fall of the Faroe-Shetland Basin: evidence from
569 seismic mapping of the Balder Formation. J. Geol. Soc. London 159, 627-630.
570
571 Smoliar, M.I., Walker, R.J., Morgan, J.W. (1996) Re – Os isotope constraints on the age of Group
572 IIA, IIIA, IVA, and IVB iron meteorites. Science 271, 1099–1102.
573
574 Stein, R., Boucsein, B. and Meyer, H. (2006) Anoxia and high production in the Paleogene central
575 Arctic Ocean: first detailed records from the Lomonosov Ridge. Geophys. Res. Lett. 33, L18606,
576 doi:10.1029/2006GL026776.

577

578 Storey, M., Duncan, R.A. and Swisher III, C.C. (2007) Paleocene-Eocene Thermal Maximum and
579 the opening of the northeast Atlantic. Science 316, 587-589.

580

581 Storey, M., Duncan, R.A. and Tegner, C. (2007) Timing and duration of volcanism in the North
582 Atlantic Igneous Province: implications for geodynamics and links to the Iceland hotspot. Chem.
583 Geol. 241, 264-281.

584

585 Svensen, H., Planke, S., Malthe-Sørenssen, A., Jamtveit, B., Myklebust, R., Rasmussen Eidem, T.
586 and Rey, S.S. (2004) Release of methane from a volcanic basin as a mechanism for initial Eocene
587 global warming. Nature 429, 542-545.

588

589 Svensen, H., Planke, S. and Corfu, F. (2010) Zircon dating ties NE Atlantic sill emplacement to
590 initial Eocene global warming. J. Geol. Soc. London 167, 433-436.

591

592 Turgeon, S.C. and Creaser, R.A. (2008) Cretaceous oceanic anoxic event 2 triggered by a
593 massive magmatic episode. Nature 454, 323-326.

594

595 Weijers, J.W.H., Schouten, S., Sluijs, A., Brinkhuis, H. and Sinninghe-Damste, J.S. (2007) Warm
596 Arctic continents during the Paleocene-Eocene Thermal Maximum. Earth Planet. Sci. Lett. 261,
597 230-238.

598

599 Wieczorek, R., Fantle, M.S., Kump, L.R. and Ravizza, G. (2013) Geochemical evidence for
600 volcanic activity prior to and enhanced terrestrial weathering during the Paleocene Eocene thermal
601 maximum. Geochim. Cosmochim. Acta, doi:10.1016/j.gca.2013.06.005

602

603 Westerhold, T., Röhl, U., Laskar, J., Raffi, I., Bowles, J., Lourens, L.J. and Zachos, J.C. (2007) On
604 the duration of magnetochrons C24r and C25n and the timing of early Eocene global warming

events: implications from the Ocean Drilling Program Leg 208 Walvis Ridge depth transect. Paleoceanography 22, PA2201, doi:10.1029/2006PA001322.

Figure captions

Figure 1: Map of locations. KR: Kheu River, Karbardino-Balkaria; DZ: Dzhengutay, Dagestan; GF: Guru-Fatima, Tajikistan; ZU: Zumaya, Spain; site numbers refer to Deep Sea Drilling Program (Sites 213 and 549) and Integrated Ocean Drilling Program (Site M0004A) cores. The shaded ellipse represents the zone of transient uplift associated with the NAIP mantle plume in the North Atlantic seaway region modelled by MacLennan and Jones (2006). Base map modified from www.scotese.com.

Figure 2: C- and Os-isotope, and Os abundance [^{192}Os] data from the Arctic and Tethys Oceans. $\delta^{13}C_{org}$ data at Site M0004A are from Stein et al. (2006), Sluijs et al. (2006) and Dickson et al. (2012). Biostratigraphic and magnetostratigraphic constraints are from Expedition 302 Scientists (2006), Backman et al. (2008), Gavrilov et al. (2003) and Gavrilov et al. (2009). F.O. *A. aug:* First occurrence of *Apectodinium augustum;* H.O. *C. w:* Highest occurrence of *Cerodinium wardense.* Dashed lines on the Site M0004A stratigraphy are used where core gaps are present. Closed symbols are repeat analyses of sample powders. $^{187}Os/^{188}Os_{(i)}$ uncertainties are the 2 S.D. external reproducibility calculated from an in-house mudrock standard. The shaded region denotes the PETM negative C-isotope excursion, based on the C-isotope stratigraphies at each location.

Figure 3: $^{187}Re/^{188}Os$-$^{187}Os/^{188}Os$ evolution plots for A, B: Site M0004A; C, D: Kheu River; E,F: Dzhengutay and G,H: Guru-Fatima. The upper row of graphs shows all data for each site, while the lower row of graphs shows only the Re-Os data from within the PETM as defined by carbon isotope stratigraphy. Regressions statistics were calculated using the long-term reproducibility (2 S.D.) of an in-house mudrock standard, which was 1.7% for $^{187}Os/^{188}Os$ and 2.5% for $^{187}Re/^{188}Os$.

Figure 4: Expanded view of C- and Os-isotope data across the onset of the PETM at Kheu River and Guru-Fatima (this study), Zumaya (Schmitz et al., 2004), and Svalbard core BH9/05 (Weiczorek et al., 2013). The four sites all record excursions of local seawater $^{187}Os/^{188}Os$ to more unradiogenic values near the onset of the PETM.

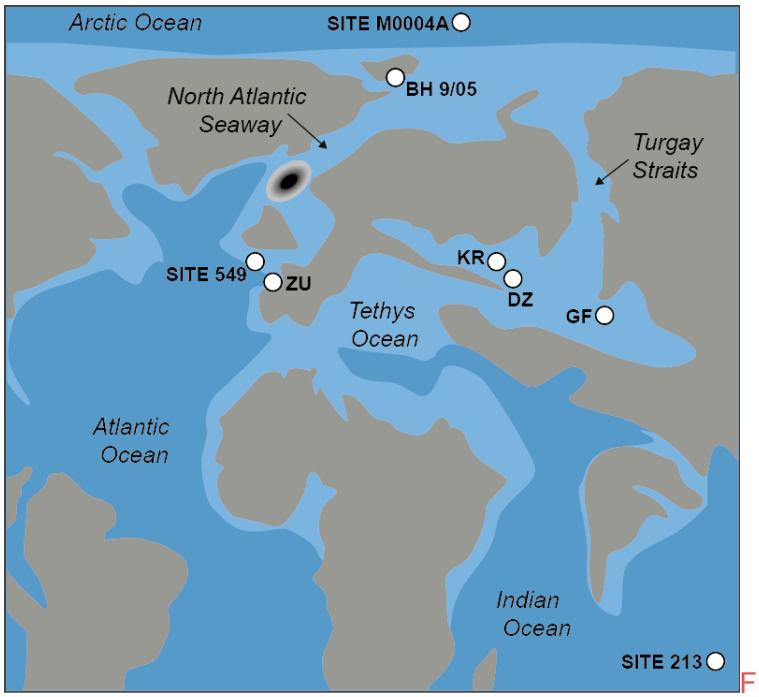

Fig. 1

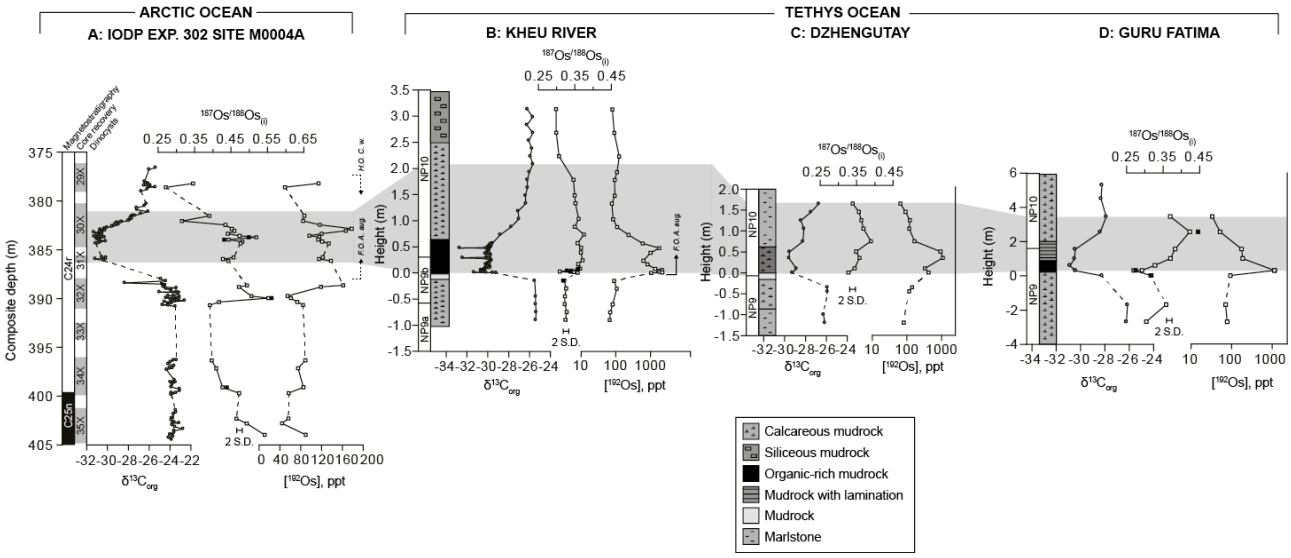

Fig. 2

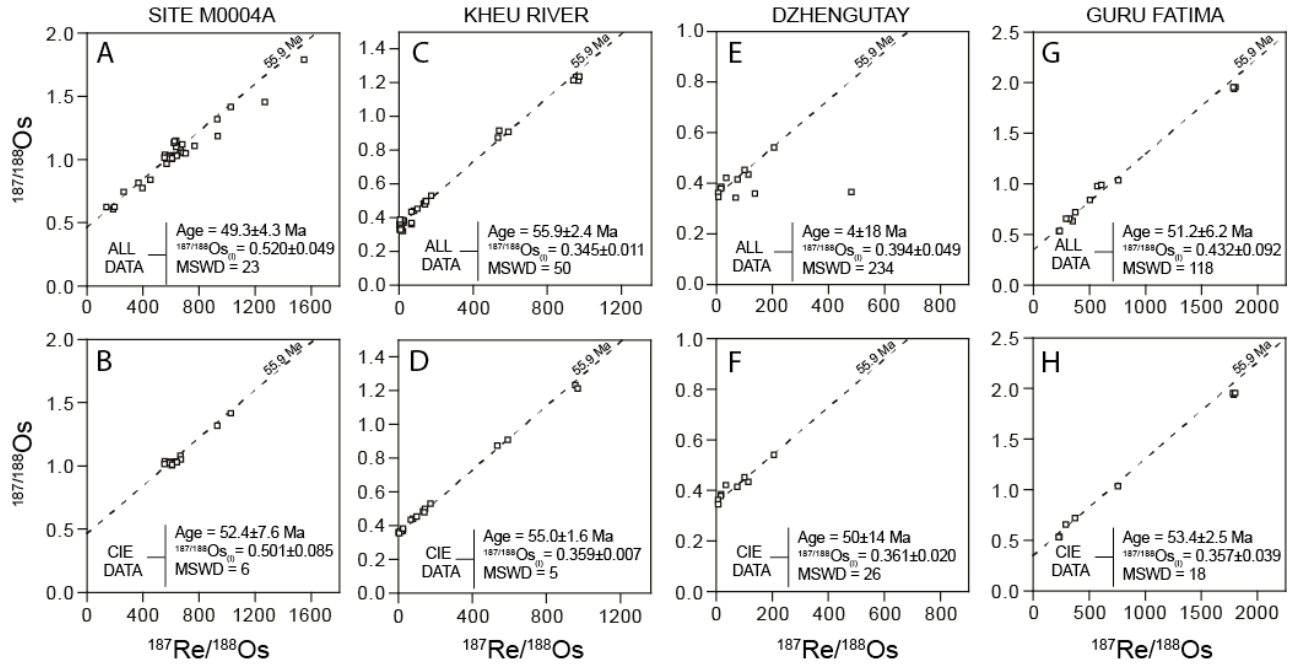
SITE M0004A
KHEU RIVER
DZHENGUTAY
GURU FATIMA
A
B
C
D
E
F
G
H
55.9 Ma
ALL DATA
CIE DATA
Age = 49.3±4.3 Ma
187/188Os(i) = 0.520±0.049
MSWD = 23
Age = 52.4±7.6 Ma
187/188Os(i) = 0.501±0.085
MSWD = 6
Age = 55.9±2.4 Ma
187/188Os(i) = 0.345±0.011
MSWD = 50
Age = 55.0±1.6 Ma
187/188Os(i) = 0.359±0.007
MSWD = 5
Age = 4±18 Ma
187/188Os(i) = 0.394±0.049
MSWD = 234
Age = 50±14 Ma
187/188Os(i) = 0.361±0.020
MSWD = 26
Age = 51.2±6.2 Ma
187/188Os(i) = 0.432±0.092
MSWD = 118
Age = 53.4±2.5 Ma
187/188Os(i) = 0.357±0.039
MSWD = 18
187/188Os
187Re/188Os

Fig. 3

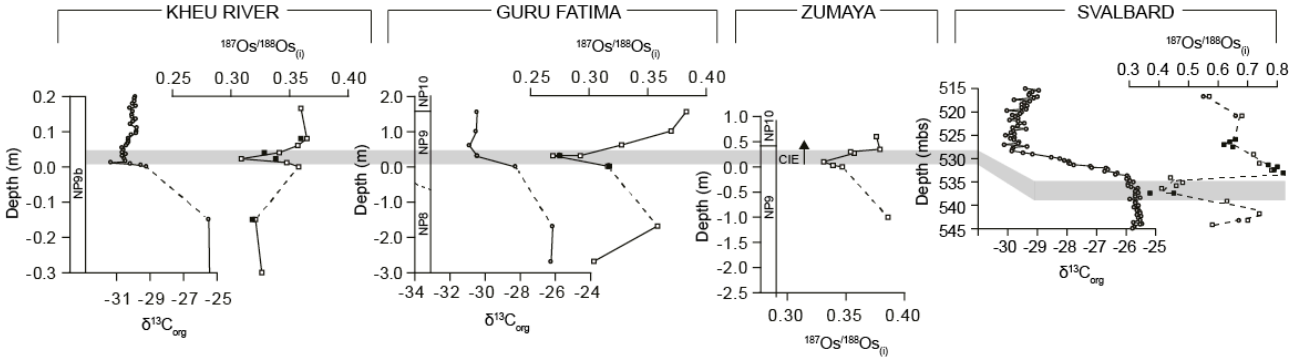
KHEU RIVER
GURU FATIMA
ZUMAYA
SVALBARD
187Os/188Os(i)
Depth (m)
Depth (mbs)
NP9b
NP10
NP9
NP8
CIE
δ13Corg

Fig. 4